Kilohertz Rotation of Nanorods Propelled by Ultrasound, Traced by Microvortex Advection of Nanoparticles

Andrew L. Balk,[†,‡,△] Lamar O. Mair,[†,‡,△,▽] Pramod P. Mathai,[†,§] Paul N. Patrone,[†,∥,⊥] Wei Wang,[#,□] Suzanne Ahmed,[#] Thomas E. Mallouk,[#] J. Alexander Liddle,[†] and Samuel M. Stavis[†,*]

[†]Center for Nanoscale Science and Technology, National Institute of Standards and Technology, Gaithersburg, Maryland 20899, United States, [‡]Maryland Nanocenter, University of Maryland, College Park, Maryland 20742, United States, [§]Department of Materials Science and Engineering, University of Maryland, College Park, Maryland 20742, United States, [∥]Institute for Research in Electronics and Applied Physics, University of Maryland, College Park, Maryland 20742, United States, [⊥]Institute for Mathematics and its Applications, University of Minnesota, Minneapolis, Minnesota 55455, United States, and [#]Department of Chemistry, The Pennsylvania State University, University Park, Pennsylvania 16802, United States. [△]A. L. Balk and L. O. Mair contributed equally to this research. [▽]Present address: Weinberg Medical Physics LLC, Bethesda, Maryland 20817, United States. [□]Present address: School of Material Science and Engineering, Shenzhen Graduate School, Harbin Institute of Technology, University Town, Shenzhen 518055, China.

ABSTRACT We measure the microvortical flows around gold nanorods propelled by ultrasound in water using polystyrene nanoparticles as optical tracers. We infer the rotational frequencies of such nanomotors assuming a hydrodynamic model of this interaction. In this way, we find that nanomotors rotate around their longitudinal axes at frequencies of up to $\approx$ 2.5 kHz, or $\approx$ 150 000 rpm, in the planar pressure node of a half-wavelength layered acoustic resonator driven at $\approx$ 3 MHz with an acoustic energy density of $< 10\ J \cdot m^{-3}$. The corresponding tangential speeds of up to $\approx 2.5\ mm \cdot s^{-1}$ at a nanomotor radius of $\approx$ 160 nm are 2 orders of magnitude faster than the translational speeds of up to $\approx 20\ \mu m \cdot s^{-1}$. We also find that rotation and translation are independent modes of motion within experimental uncertainty. Our study is an important step toward understanding the behavior and fulfilling the potential of this dynamic nanotechnology for hydrodynamically interacting with biological media, as well as other applications involving nanoscale transport, mixing, drilling, assembly, and rheology. Our results also establish the fastest reported rotation of a nanomotor in aqueous solution.

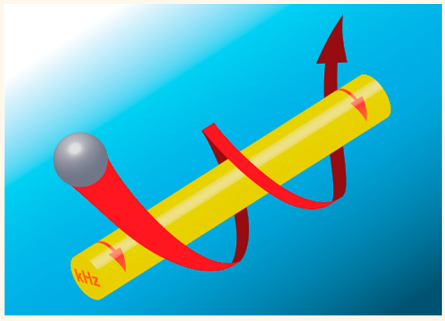

KEYWORDS: acoustic · microvortex · nanomotor · nanoparticle · nanorod · rotation · ultrasonic · ultrasound

Nanorods propelled by ultrasound[1] were recently discovered as a dynamic nanotechnology with emerging biomedical applications.[2] In contrast to chemically,[3−6] magnetically,[7,8] or electrically actuated nanomotors,[9] acoustically actuated nanomotors can transport through aqueous solutions with high ionic strengths and without toxic fuels or external magnetic or electric fields. Such nanomotors can be readily used in living tissue[10] and in combination[11] with other propulsion mechanisms[12] and have been envisioned[13,14] for use in exciting applications such as diagnosing disease,[15,16] delivering drugs,[17] and performing surgery.[18] However, to fulfill the potential of nanomotors propelled by ultrasound for rapidly transporting through and strongly interacting with biological media, the basic dynamics of the nanomotors must be clearly understood.

Such nanomotors, which are typically metallic rods that are a few micrometers in length and a few hundred nanometers in diameter, exhibit several modes of motion in the presence of acoustic actuation. Both translation along and rotation around the principal longitudinal axis (henceforth, translation and rotation) of single nanomotors have been observed, as well as collective motions involving many interacting nanomotors.[2] While translation is an interesting mode of motion that is relatively straightforward to directly measure, rotation is a particularly fascinating mode of motion that motivates further study, for several reasons. First, hydrodynamic interactions of nanomotors with other objects or one another at low Reynolds number (*Re*) are determined in part by the vortical flows around nanomotors, which relate to the rates of nanorod rotation.[19] Interactions

* Address correspondence to samuel.stavis@nist.gov.

Received for review May 20, 2014 and accepted July 7, 2014.

Published online July 14, 2014
10.1021/nn502753x

among multiple nanomotors[2] may be strongly influenced by such microvortices, depending on the rotation and flow rates. Second, any correlation, or lack thereof, between rotation and translation is important for understanding, engineering, and applying these modes of motion. The deliberate coupling of rotation and translation may provide a mechanism for propulsion, as is the case for natural[20] and artificial[21] flagella, while the deliberate decoupling of rotation and translation may enable independent control over these modes of motion, as is generally necessary for selective transport and rotary tools. Third, rotation is difficult to directly image for nanomotors that are rapidly rotating and optically featureless around the longitudinal axis, so that rates of rotation are quantitatively unknown and *potentially* very high, considering the ultrasonic actuation frequency of a few megahertz. Therefore, the extent of hydrodynamic interaction with the surrounding environment and any correlation of the modes of motion are open problems. For these reasons, measuring hydrodynamic interaction and inferring rotational motion are essential to understanding and using this dynamic nanotechnology.

Here, as illustrated in Figure 1, we use polystyrene nanoparticles as optical indicators of the microvortical flows around gold nanorods propelled by ultrasound in an acoustic resonator. We track the microvortex advection of nanoparticle tracers around rotating and translating nanomotors by dark-field localization microscopy. We input our measurements of this motion into a hydrodynamic model to infer the rotational frequencies of the nanomotors. We discuss simplifying assumptions underlying our analysis and resulting uncertainties that are relevant both to our measurements and to future applications of nanomotors. In the planar pressure node of a half-wavelength layered acoustic resonator driven at $\approx$ 3 MHz with an energy density of < 10 J·m^{-3}, we infer that nanomotors rotate at frequencies of up to $\approx$ 2.5 kHz, or $\approx$ 150 000 rpm. This establishes the fastest reported rotation of a nanomotor in aqueous solution and corresponds to tangential speeds at nanomotor surfaces of up to $\approx$ 2.5 mm·s^{-1}, which are 2 orders of magnitude faster than translational speeds of $\approx$ 20 μm·s^{-1}. We find that rotation and translation are independent and variable modes of motion within experimental uncertainty. These surprising results are essential to understanding the behavior of nanomotors propelled by ultrasound, and this unprecedented combination of small size and fast rotation is highly relevant to emerging biomedical applications of nanomotors, as well as other applications involving nanoscale transport,[22] mixing,[23] drilling,[24,25] assembly,[26] and rheology.[27]

RESULTS AND DISCUSSION

Motivation. Acoustic actuation is a popular method for manipulating small objects in liquids,[1] and the recent discovery of the propulsion of metallic nanorods by ultrasound[2,12,28] has generated growing interest in the use of such nanomotors for interacting with biological media. However, the basic dynamics of these nanomotors and the resulting hydrodynamic interactions between nanomotors and other small objects are not clearly understood. Such dynamics and interactions may be probed by imaging the motion of tracer particles and thus visualizing the flow fields around objects of interest. Flow fields around motile bacterial swimmers have been studied[29,30] in this way to better understand swimming mechanisms and hydrodynamic interactions between bacteria. Inspired by natural swimmers,[31] artificial motors have been recently developed[7,21] for inducing fluid flows and transporting bacteria and other microscale objects by hydrodynamic interactions.[32] However, controlling and measuring dynamics and interactions at low *Re* becomes increasingly challenging as the dimensions of nanoscale objects become less uniform and as the motion of nanoscale objects becomes more stochastic.[6] Our multidisciplinary study therefore combines ultrasonic actuation, low *Re* fluid dynamics and hydrodynamic interactions, nanoscale control and fluctuations, and measurement science in an approach toward understanding the behavior of this dynamic nanotechnology.

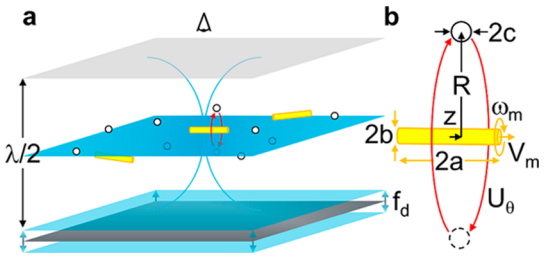

Figure 1. Schematics illustrating the acoustic actuation of a nanomotor and the microvortex advection of a nanoparticle. (a) A half-wavelength layered acoustic resonator filled with water is driven at a frequency $f_d \approx 3$ MHz with an energy density of < 10 J·m^{-3}. Gold nanorods are levitated into and propelled around the planar pressure node of the resonator. Polystyrene nanoparticles are levitated into the planar pressure node and advected by the microvortical flows around nearby nanomotors. (b) We model a nanomotor as a cylinder of length 2*a* and diameter 2*b* with the longitudinal axis oriented in the focal plane of an optical microscope. The nanomotor rotates around the longitudinal axis with an angular speed of $\omega_m = 2\pi f_m$ and translates along the longitudinal axis with a speed V_m. We model the nanoparticle as a sphere of diameter 2*c* and diffusivity *D*, located at a radial distance *R* from the nanomotor and at a fore and aft position *z* from the center along the longitudinal axis of the nanomotor. The nanoparticle is advected with a tangential speed U_θ.

Analytical Approach. We measure the microvortex advection of a tracer nanoparticle around a nanomotor, input our measurements into a hydrodynamic model of this interaction, and in this way infer the rotational frequency of the nanomotor. Our approach relies on several simplifying approximations—including that of a Stokes flow around a nanomotor, that only hydrodynamic forces from a microvortical flow act on a

nanoparticle, and that nanomotors and nanoparticles are, respectively, perfectly cylindrical and spherical in shape—and thus ignores a description of the actual cause of such motion. We describe and justify these simplifying assumptions in the Supporting Information. A complete theoretical model of the acoustic actuation of nanomotor rotation and translation is beyond the scope of our study. However, the eventual development of such a model must be consistent with our novel experimental results. In particular, we measure a relation between the tangential speed of a nanoparticle advecting around a rotating nanomotor and radial distance between the pair that is reasonably well described by a hydrodynamic interaction,[19] which must be explained by any, more detailed, model of the system.

Microvortical Flow. We use an analytical expression derived by Chwang and Wu[19] to model the vortical flow at low *Re* around a slender axisymmetric body rotating around its longitudinal axis. The following expression applies in the limiting case of a long rod, which is a good approximation for our experimental nanorod length to diameter aspect ratio of ≈ 7, as shown in Figure 2. If the measured tangential speed of the vortical flow as indicated by a tracer nanoparticle is U_θ, then

$$U_\theta \approx \frac{\omega_m b^2}{2R}\left[\frac{z+a}{\sqrt{(z+a)^2+R^2}} - \frac{z-a}{\sqrt{(z-a)^2+R^2}}\right] \quad (1)$$

The other variables in this expression are as follows: ω_m is the inferred angular speed of the nanomotor, which we also discuss as a rotational frequency $f_m = (\omega_m/2\pi)$; R is the measured radial distance between the center of a tracer nanoparticle and the center of a nanomotor; z is the measured fore and aft position of the tracer nanoparticle from the center along the longitudinal axis of the nanomotor; and $2a$ and $2b$ are the measured length and diameter of the nanomotor, respectively. This expression is independent of viscosity in the limit of a quasi-static Stokes flow. This model has been experimentally validated for objects with dimensions on the order of hundreds of micrometers[33] and is further tested for the rotating nanomotors studied here. Nanomotor translation also induces a flow field, which we estimate to be relatively insignificant, while *a posteriori* estimates of *Re* and viscous penetration depth are consistent with our assumption of a quasi-static Stokes flow, as described below and in the Supporting Information.

Tracer Considerations. We trace the flow field around a nanomotor by imaging the microvortex advection of a nanoparticle. The size of the nanoparticle and proximity to the nanomotor must be chosen such that the nanoparticle serves as both a passive and precise indicator of the flow field. Several competing experimental considerations inform our semi-empirical selection of a nanoparticle hydrodynamic radius of $c \approx 200$ nm and radial distance of $R > 1\ \mu$m. The flow field is perturbed less by a smaller nanoparticle that is farther from the nanomotor. Conversely, a larger nanoparticle that is closer to the nanomotor exhibits less stochastic diffusion and is advected more deterministically. A larger nanoparticle also scatters more light in dark-field microscopy and can be localized more precisely.

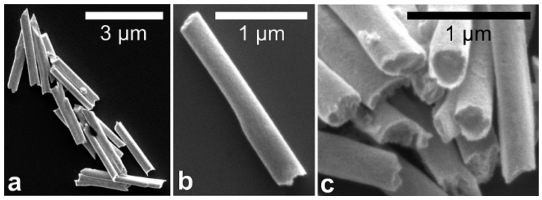

Figure 2. Scanning electron micrographs showing the sizes and shapes of gold nanorods. (a) The ensemble of nanorods has lengths of $2a = (2.19 \pm 0.28)\ \mu$m and diameters of $2b = (316 \pm 39)$ nm (average $\pm$ standard deviation, $N = 20$), yielding an average length to diameter aspect ratio of ≈ 7. (b) Individual nanorods show variation in diameter, (c) end shape and surface roughness.

The maximum size and minimum proximity of a tracer nanoparticle is limited by the fractional hydrodynamic perturbation to the nanomotor rotation from the wake of a nanoparticle, $\delta_f = |((f_0 - f_{pert})/f_0)|$, where f_{pert} and f_0 are, respectively, the perturbed and unperturbed nanomotor rotational frequencies. We estimate a range of values for δ_f using two far-field approximations, both based on a single iteration of the method of reflections.[34] Details of these calculations are presented in the Supporting Information. In a deliberate overestimate of the perturbation, we artificially impose an external force to hold a nanoparticle stationary in the flow field described by eq 1, and we calculate the perturbation from this additional Stokes drag. In the far field, the actual perturbation is smaller than this overestimate, which yields a perturbation of $\delta_f < 2\%$ for $R > 1\ \mu$m, as shown in Figure S1. This analysis is informative for emerging applications of nanomotors hydrodynamically interacting with other small objects, such as cellular organelles,[10] that may be constrained in a biological media. In a realistic estimate of the perturbation, with no external forces and torques, the fluid flow incident on an ideal tracer will, in the Stokes approximation, transport the tracer with the same velocity and angular velocity as the average flow field at the tracer.[9] In this case, we treat the perturbation δ_f as being due only to nanoparticle rotation, using the approximation of a tracer in a linearly varying velocity flow field in the radial direction. This analysis yields a perturbation of $\delta_f < 0.5\%$ for $R > 1\ \mu$m, as shown in Figure S1, which is negligibly small compared to the other sources of uncertainty in our measurements described below. Therefore, the nanoparticles qualify as effectively noninteracting tracers of microvortical flows in our study.

Conversely, the minimum size and maximum distance of a tracer nanoparticle are limited by the stochastic diffusion of a nanoparticle, contributing

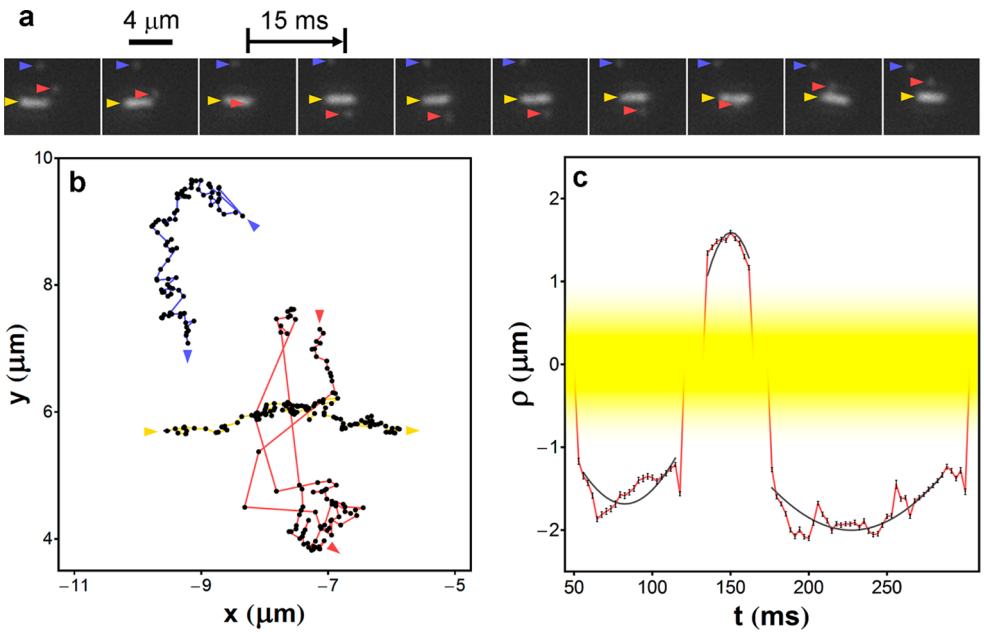

Figure 3. Representative data showing the measurement and analysis of the motion of a nanomotor and two nanoparticles. (a) Dark-field micrographs showing projections in the image plane of nanoparticle diffusion as indicated by blue arrows, nanomotor propulsion as indicated by gold arrows, and nanoparticle advection for $\approx 2\pi$ radians as indicated by red arrows. Sequential video frames are advanced in time by $\approx$ 15 ms from left to right. (b) Nanomotors and nanoparticles localized in each video frame. Sequential data points are advanced in time by $\approx$ 3 ms, and trajectories in the camera coordinate frame are plotted as color-coded lines with arrows indicating the direction of motion. (c) The trajectory of the nanoparticle is transformed into the coordinate frame of the nanomotor. Projected radial distance ρ as a function of time t is modeled as a sinusoidal function, shown as a gray line, to extract tangential speed U_θ and radial distance R between multiple frames of a video. The nanomotor obscures the nanoparticle around $\rho \approx 0$, as indicated by the gold blur. Vertical and horizontal bars are one standard uncertainty and are smaller than the data points in some cases.

uncertainty to a measurement of the deterministic advection of the nanoparticle by the flow field and thus U_θ and R. A nanoparticle is useful as a tracer in our measurements only if the rate of advection significantly exceeds the rate of diffusion. The relative rates of advection and diffusion are compared by the Brenner number, $Br = U_\theta R/\pi D$, where D is the measured diffusion coefficient of the nanoparticle tracer, expressed through the Stokes–Einstein relation as $D = k_B T/6\pi\eta c$, where k_B is the Boltzmann constant, T is the absolute temperature of the aqueous solution, and η is the dynamic viscosity. Due to the fast microvortical flows around nanomotors, we measure typical values of $Br \gtrsim 10$ and a typical relative standard uncertainty in U_θ of < 5%, quantifying our extent of hydrodynamic control over the transport of nanoparticles and satisfying our need for quasi-deterministic nanoparticle transport in our measurements.

Independent Motions. In the absence of acoustic actuation, polystyrene nanoparticles randomly diffuse throughout the sample volume, while gold nanorods randomly diffuse and eventually sediment onto the matching layer of the acoustic resonator. In the presence of acoustic actuation, both polystyrene nanoparticles and gold nanorods levitate into and concentrate around the planar pressure node of the acoustic resonator,[35] as illustrated in Figure 1. Polystyrene nanoparticles continue to diffuse randomly and are advected to varying extents, possibly by acoustic streaming, around the planar pressure node of the resonator. Independently of interactions with nanomotors, nanoparticles diffuse at the same rate of $D = (1.04 \pm 0.14)\ \mu m^2 \cdot s^{-1}$ (average $\pm$ standard uncertainty) before, during, and after acoustic actuation. Individual gold nanorods are propelled throughout the planar pressure node of the acoustic resonator with significant variation in translational speed, path, and concentration, as demonstrated previously.[2] Figure 3 shows representative data of nanoparticle diffusion, nanomotor propulsion, and nanoparticle advection.

Microvortex Advection. Previously, microvortical flows among ensembles of nanomotors and nanoparticles were *qualitatively* observed.[2] Here, we *quantitatively* analyze the microvortex advection of single nanoparticles around single nanomotors propelling randomly past, as shown in Figure 3 and in Video S1. Absent a nearby nanomotor, nanoparticles diffuse randomly and exhibit minimal advection by acoustic streaming. Importantly, we observe the microvortex advection of nanoparticles *only* as nanomotors transit in close proximity, and we do not observe the microvortex advection of nanoparticles without a nanomotor nearby. These observations demonstrate that the microvortex advection of a nanoparticle is a result of the hydrodynamic interaction with a nanomotor and is not a result of any primary acoustophoretic streaming field

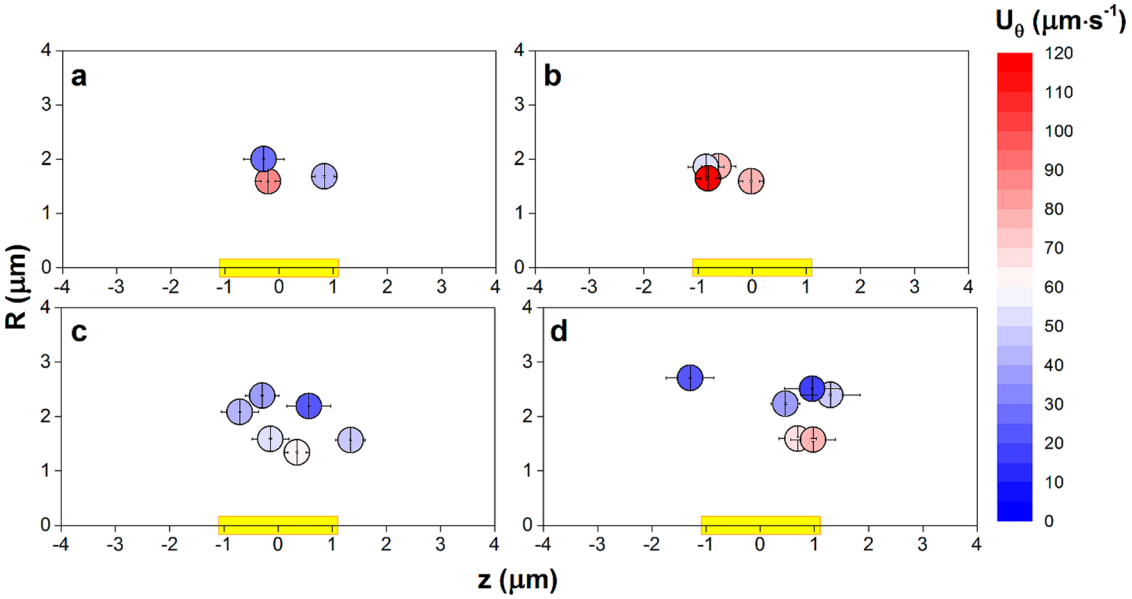

Figure 4. Representative data showing four microvortex advection events of varying speed and increasing persistence. The data points in (a) correspond to the nanomotor shown in Figure 3, while the data points in (b), (c), and (d) correspond to other nanomotors. Variation in the ranges of tangential speed U_θ indicates different microvortical flow speeds around the individual nanomotors driven by different rotational frequencies f_m. Nanoparticles are shown to scale and color coded to U_θ, with 5 μm·s^{-1} gradations in color conservatively representing the standard uncertainty of U_θ. Vertical and horizontal bars are one standard uncertainty of radial distance R and one standard deviation of fore and aft position z, respectively, as nanomotors translate and diffuse along the longitudinal axis during microvortex advection. Nanorods are illustrated approximately to scale.

in the acoustic resonator, as described in the Supporting Information. The microvortex advection of nanoparticles is evident in the majority of close encounters with nanomotors, indicating that most of these nanomotors have associated microvortical flows. However, due to the large distribution of approach distances between individual nanomotors and nanoparticles, particle tracking in three dimensions is needed to quantify the fraction of rotating nanomotors. We categorize microvortex advection for analysis by the persistence of nanoparticle entrainment, measured in units of radians around the longitudinal axis. While some advection events persist for $< \pi$ radians, others persist for up to $\approx 8\pi$ radians, as shown in Video S2. This variability in persistence is due to the stochastic diffusion of both nanomotors and nanoparticles, as well as variation in approach distances and translational and rotational speeds of nanomotors, as described below. We quantitatively analyze only those nanoparticles entrained in a microvortex for $\geq 2\pi$ radians, as shown in Figure 3a, as such events allow for more reliable tracking of nanoparticle motion. Highly persistent microvortex advections enable repeated measurements of the rotation of individual nanomotors and are therefore particularly interesting for quantitative analysis.

We extract values of U_θ, R, and z from each microvortex advection event of $\geq 2\pi$ radians, as shown in Figure 3 and Figure S3. We assume constant values of U_θ and R during a circular trajectory of a nanoparticle around a nanomotor, occurring at large enough Br. Details of this analysis are described in the Methods and in the Supporting Information. Figure 4 shows these measured quantities from the increasingly persistent microvortex advection of four nanoparticles around four nanomotors. The data points in Figure 4a correspond to the nanomotor shown in Figure 3 and in Video S1, while the data points in Figure 4b–d correspond to other nanomotors. Each microvortex advection event is plotted to the scale of the nanoparticles and color coded to U_θ, with 5 μm·s^{-1} gradations in color conservatively representing the standard uncertainty in U_θ. Variations in z are due to nanomotor propulsion and diffusion along the longitudinal axis, as well as diffusion of nanoparticles, during microvortex advection. U_θ varies over different ranges for the four nanomotors, indicating variation in microvortical flow rates but making it difficult to discern a trend in Figure 4 and motivating additional testing of our measurement method before returning to an analysis of the rates of rotation of individual nanomotors. We analyze a total of nine individual nanomotors to obtain 41 total individual microvortex advections.

Model Test. We test the validity of eq 1 to infer values of $\omega_m = 2\pi f_m$ from our experimental measurements. To do so, we fit the experimental relation between *all* measurements of U_θ and R to eq 1, using average values of a, b, and z, while leaving ω_m as a free parameter. The fit has an adjusted $R^2 = 0.86$ and is shown as a gray line in Figure 5, demonstrating reasonable agreement between the expected $U_\theta(R)$ relation and the ensemble experimental data and, in this way, supporting our use of a hydrodynamic model of the interaction between a nanomotor and a nanoparticle.

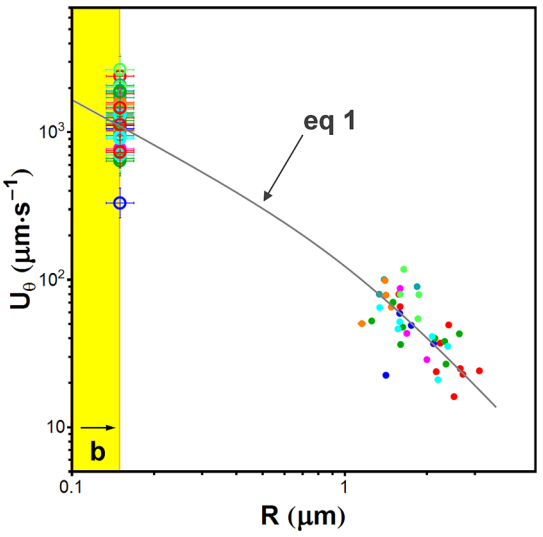

Figure 5. We test the validity of eq 1 to infer nanomotor rotational frequency from the microvortex advection of tracer nanoparticles. We fit the experimental relation between tangential speed U_θ and radial distance R to eq 1, using average values of length $2a$, diameter $2b$, and fore and aft position z, while leaving angular speed $\omega_m = 2\pi f_m$ as a free parameter. The fit has an adjusted $R^2 = 0.86$ and is shown as a gray line, demonstrating reasonable agreement between theory and experiment. Repeated measurements of the persistent microvortex advection of tracer nanoparticles around individual nanomotors are color coded. Individually inferred values of f_m and derived nanomotor surface tangential speeds, shown as open circles, are consistent with the fit relation from the ensemble experimental data. Vertical and horizontal bars are one standard uncertainty and may be smaller than the data points.

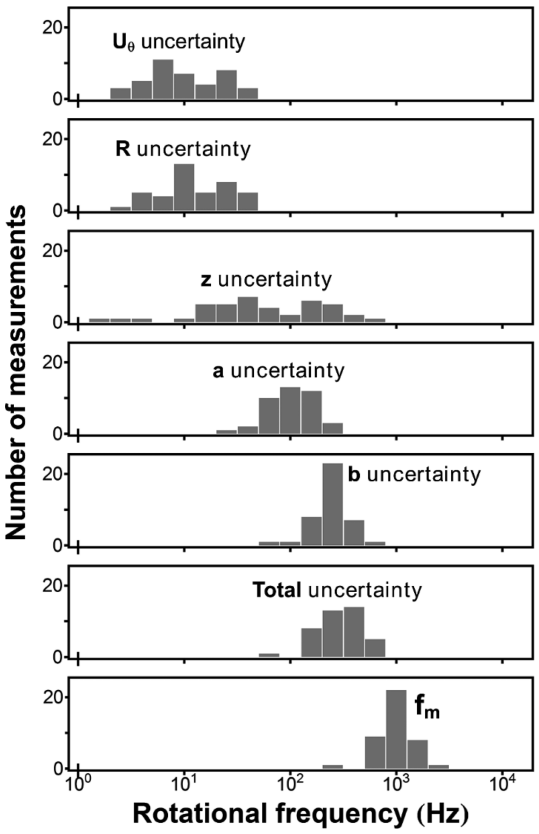

Figure 6. An analysis of measurement uncertainty elucidates our inferences of kilohertz rotation and informs future applications of nanomotors. Each of the five measured values input into eq 1 contributes differently to the total uncertainty in rotational frequency f_m. The various contributions are plotted as histograms, in the case where nanomotor length $2a$ and diameter $2b$ are characterized as an ensemble average and standard deviation. The distributions of nanorod length, $2a$ = (2.19 ± 0.28) μm, and nanorod diameter, $2b$ = (316 ± 39) nm (average ± standard deviation, N = 20), result in >85% of the total uncertainty in f_m, demonstrating that dimensional control is critical in future applications of nanomotors.

Significant scatter of the data is evident, resulting from variation in the rotational frequencies and dimensions of individual nanomotors, and in fore and aft position during microvortex advection due to nanomotor diffusion and propulsion. The left side of Figure 5 shows tangential surface speeds at the average nanomotor radius of $b \approx 160$ nm for individual microvortex advection events, as inferred using eq 1. These individually inferred values, with an average tangential surface speed of ≈ 1.5 mm·s^{-1}, are consistent with the fit relation from the ensemble experimental data.

Uncertainty Propagation. Each of the five variables that we input into eq 1, U_θ, R, z, a, and b, has an associated uncertainty that is propagated through to the inferred value of ω_m. It is worth examining the relative importance of these uncertainties for the purposes of better understanding our inference of rotational frequency and of informing future applications of nanomotors. We begin by inputting into eq 1 average values of $2a$ and $2b$ with standard deviation values obtained from scanning electron microscopy treated as measurement uncertainties on an ensemble basis. Figure 6 shows, in this case, the resulting contributions of each of the five variables to the total uncertainty in $f_m = \omega_m/2\pi$ as histograms. It is apparent from Figure 6 that if the lengths and diameters of nanomotors cannot be characterized on an individual basis, as is the case for our experimental study and presumably for many applications of nanomotors, then the statistical distributions of these values dominate the uncertainty in an inference of nanomotor rotation, accounting for > 85% of the total uncertainty. The polydispersity in nanorod dimensions, $2a$ = (2.19 ± 0.28) μm and $2b$ = (316 ± 39) nm (average ± standard deviation, N = 20), is a result of the electrodeposition process guided by a nanoporous template that we use to fabricate the gold nanorods, emphasizing that nanoscale dimensional control over nanorod structure is critical in future studies and applications of nanomotors. As a final note on the propagation of measurement uncertainty, the relatively small contribution of U_θ and R to the total uncertainty in an estimate of f_m validates our semi-empirical selection of tracer nanoparticle size and proximity.

Rotation Inference. With our hydrodynamic model tested and our measurement uncertainty characterized, we analyze our inferences of the rotation of individual nanomotors. We study, for example, the

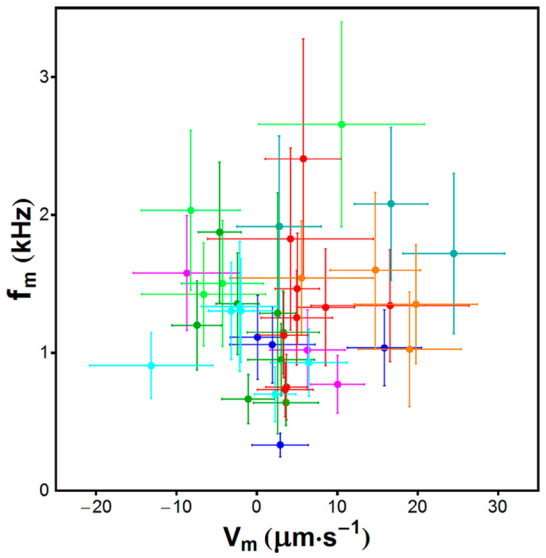

Figure 7. Nanomotor rotation and translation are independent and variable modes of motion. Individual nanomotors are coded by different colors maintained from Figure 5. The resulting data points are scattered with rotation and translation uncorrelated, even for an individual nanomotor during persistent microvortex advection. Vertical and horizontal bars are one standard uncertainty. Uncertainty in rotational frequency f_m is dominated by the polydispersity of nanorod dimensions, while uncertainty in translational speed V_m is dominated by diffusion along the longitudinal axis of the nanomotors.

persistent microvortex advection of tracer nanoparticles around the two nanomotors shown in Figure 4c and d. Individual estimates of rotational frequency and measurement uncertainty, as well as the statistical variation of these values, are tabulated in Table S1 of the Supporting Information. Differences between repeated inferences of the rotational frequency of an individual nanomotor over a time scale of ≈ 100 ms are often within, but occasionally exceed, the measurement uncertainty. Similarly, the variation in rotational frequency between different nanomotors exceeds the measurement uncertainty in some instances. Differences between the rotational frequencies of individual nanomotors may be attributed to heterogeneity in nanomotor structure and the resulting transduction of acoustic energy into motion, as well as any lateral variation in acoustic energy density around the planar pressure node of the acoustic resonator. Nanomotors rotate with a broad distribution of inferred frequencies ranging from $f_m \approx$ (0.5 to 2.5) kHz, as shown in Figure 6. For nanorods with radii of $b \approx 160$ nm, these inferred rotational frequencies correspond to Reynolds number $Re < 10^{-3}$ and viscous penetration depths of > 8 μm, which are consistent with our assumption of a quasi-static Stokes flow,[36] as described in the Supporting Information.

Rotation and Translation. We compare inferred rotational frequencies f_m to measured translational speeds V_m of individual nanomotors during the microvortex advection of tracer nanoparticles. We analyze the correlation between f_m and V_m to determine if rotation and translation are dependent or independent modes of motion. It seems evident in Figure 7 that rotation and translation are independent and variable. Noting that we do not know the direction of nanomotor rotation or the polarity of any coupling between rotation and translation, we calculate adjusted R^2 values for $f_m(|V_m|)$ such that our analysis is sensitive to any existing correlation. We find an adjusted R^2 value for $f_m(|V_m|)$ that is similar to that of randomly generated data, demonstrating that, within the uncertainty of our measurements, rotation and translation are independent modes of motion in our experimental system.

CONCLUSIONS

The field of nanomotors propelled by ultrasound is rapidly developing, so that understanding the dynamics and interactions of these devices is becoming increasingly important for advancing novel applications and understanding potential limitations. Our study provides the first measure of the microvortical flows around rotating and translating gold nanorods propelled by ultrasound. We input our measurements into a simplified hydrodynamic model to infer the rotational frequencies of nanomotors. In the planar pressure node of a half-wavelength layered acoustic resonator driven at ≈ 3 MHz and with an energy density of < 10 J·m^{-3}, we infer that gold nanorods rotate around the longitudinal axis at frequencies of up to ≈ 2.5 kHz, or ≈ 150 000 rpm, corresponding to tangential surface speeds of up to ≈ 2.5 mm·s^{-1}. This is the fastest reported rotation of a nanomotor in aqueous solution, exceeding a recently reported record value[9] by an order of magnitude. Nanomotors also translate along the longitudinal axis at speeds of up to ≈ 20 μm·s^{-1} in our experimental system. The even faster translation of up to $V_m \approx 200$ μm·s^{-1} of similar nanomotors in a previous study is likely due to the use of an acoustic resonator with a similar input power but a higher quality factor,[2] indicating the possibility of nanomotor rotation faster than ≈ 2.5 kHz. We find that the majority of randomly propelling nanomotors have associated microvortical flows, independently of translational speed or coupling between nanomotors.

These results suggest several future studies. We hypothesize that microvortical flows could mediate the attraction or repulsion of multiple nanomotors in a manner that is analogous to the interaction of magnetic fields resulting from multiple magnetic dipoles, due to the similarity of the underlying equations. Future study is required to test our hypothesis, as well as to clarify the actuation mechanisms for rotation and translation. Precisely nanofabricated structures, combined with the measurement methods and results that we report here, would be helpful in this regard. The longitudinal asymmetries of the concavity of the ends of a nanorod and of the angle of a nanorod relative to the planar pressure node have been implicated in nanomotor

translation[2,12] and rotation,[2] respectively. The kilohertz rotation of nanomotors indicates that axial asymmetry, in particular helicity, is a relevant structural characteristic to further control and investigate. Interestingly, rotation and translation are *not* coupled through any helicity of our nanorods, indicating different acoustic actuation mechanisms driving the two modes of motion and suggesting the future possibility of deliberately decoupling and separately controlling rotation and translation. Beyond the basic issue of selectively transporting nanomotors by translation and inducing microvortical flows by rotation, decoupling rotation and translation is essential in future applications of nanomotors as rotary tools, which generally require independent control over speed and feed. Conversely, recent reports of the fabrication and actuation of metallic helices with dimensions that are similar to our nanorods also suggest the future possibility of deliberately coupling rotation and translation propelled by ultrasound.[7,21,37−41]

This unprecedented combination of small size and fast rotation could lead to important advances in biomedical and other applications of nanomotors propelled by ultrasound. For example, our results quantify how nanomotors with associated microvortical flows can quasi-deterministically control the transport of other objects by rapid advection, despite the high rates of stochastic diffusion of nanoscale objects. The enhanced mixing of liquids at low Re[23] follows naturally from our results, while nanoscale drilling, assembly,[26] and rheology[27] are also possibilities with nanomotor rotation occurring at kilohertz frequencies. However, our measurements also show that future applications would be limited by precise control over the nanoscale dimensions of individual nanomotors. Moreover, our results indicate that such applications should not be predicated on assumed steady-state motion or correlation between the rotation and translation of nanomotors.

METHODS

Acoustic Resonator. We perform our experiments in a half-wavelength layered acoustic resonator. A ceramic piezoelectric transducer with a thickness of ≈ 620 μm and a diameter of ≈ 12 mm is adhered by an epoxy coupling layer with a thickness of (9 ± 4) μm (average ± standard deviation) to the unpolished back side of a silicon matching layer with a thickness of (430 ± 1) μm (average ± standard deviation), a width of ≈ 20 mm, and a length of ≈ 25 mm. A polydimethylsiloxane (PDMS) gasket with a thickness of ≈ 250 μm, a width of ≈ 5 mm, and a length of ≈ 10 mm is reversibly bonded to the polished front side of the silicon matching layer, setting the fluid layer thickness. The resonator volume of ≈ 0.8 μL is formed by a circular hole with a diameter of ≈ 2 mm in the PDMS gasket, into which the sample solution is pipetted. A borosilicate coverslip with a thickness of ≈ (160 to 190) μm and a width and length of ≈ 18 mm is reversibly bonded to the top of the PDMS gasket as the reflecting layer. We drive the piezoelectric transducer with a sinusoidal function of amplitude from (5 to 10) V and frequency from (2.75 to 3.10) MHz. The conditions for forming a standing wave in the resonator are described by

$$t_{fl} = \frac{1}{2}n\lambda = \frac{1}{2}n\left(\frac{c_w}{f_d}\right) \quad (2)$$

where t_{fl} is the thickness of the fluid layer, n is the number of nodes, λ is the wavelength of sound in the fluid, c_w is the speed of sound in water, and f_d is the driving frequency of the piezoelectric transducer. For a layered resonator with a single node operating at values of f_d from (2.75 to 3.10) MHz, the ideal value of t_{fl} respectively varies from (240 to 270) μm. We tune f_d for each experiment to accommodate variation in PDMS gasket thickness and borosilicate coverslip thickness. We measure an electrical input power of < 1 W over the entire piezoelectric transducer area of 113 mm^2. In the presence of acoustic actuation, nanomotors and nanoparticles levitate into a band with a thickness of several micrometers near the vertical midplane of the resonator, with nanomotors typically oriented with the longitudinal axis in this plane.

Nanorod Properties. We fabricate gold nanorods by an electrodeposition process guided by a nanoscale porous alumina template.[42] We characterize the sizes and shapes of individual nanorods by scanning electron microscopy, as shown in Figure 3. The nanorods, as an ensemble, have dry diameters of (316 ± 39) nm and lengths of (2.19 ± 0.28) μm (average ± standard deviation, N = 20), with individual nanorods showing variation in end shape and surface roughness. We load gold nanorods into the sample cell at a volume fraction of ≈ 10^{-5}.

Nanoparticle Properties. We use polystyrene spheres with wet diameters of (390 ± 12) nm (average ± standard deviation, as measured by the manufacturer using a disc centrifuge; the average value is traceable to the National Institute of Standards and Technology) to trace the flow fields induced by rotating nanomotors. Such nanoparticles serve as good tracers for several reasons beyond the considerations discussed above guiding our selection of nanoparticle size. While an ideal tracer would have the same density as water, polystyrene is only ≈ 5% denser than deionized water, and such nanoparticles can be obtained commercially with nearly monodisperse size distribution, highly regular spherical shapes, and relatively smooth surfaces. We load polystyrene nanoparticles into the sample cell at a volume fraction of ≈ 10^{-5}.

Optical Microscopy. We image the motion of nanomotors and nanoparticles by dark-field microscopy. To balance collection efficiency, field of view, and depth of field, we use an air immersion objective lens with corrections for flat field and chromatic aberrations, a magnification of 50×, and a numerical aperture of 0.80. The depth of field of ≈ 1.2 μm is collocated with the planar pressure node of the acoustic standing wave near the vertical midplane of the acoustic resonator. The polished front side of the silicon matching layer provides low background light scattering for high optical signal-to-noise ratio. Images are collected at a frame rate of ≈ 338 s^{-1} using a scientific complementary metal−oxide−semiconductor (sCMOS) camera with an on-chip pixel size of 6.5 μm. Videos are typically acquired in 8 × 10^3 frame segments composed of 5 × 10^2 initial frames immediately before acoustic actuation, 7 × 10^3 intermediate frames during acoustic excitation, and 5 × 10^2 final frames immediately after acoustic excitation.

Motion Analysis. We analyze the motion of nanomotors and nanoparticles by modeling the two-dimensional images of three-dimensional objects and motions, localizing and orienting nanomotors and nanoparticles within video frames, and tracking the motion of nanomotors and nanoparticles between video frames.

Nanomotors and nanoparticles are first localized within each video frame, and frames showing interactions between nanomotors and nanoparticles are spatially and temporally cropped. A region of interest (ROI) is centered around a nanomotor as the brightest and largest feature within the ROI. This feature is fit to four spatially offset error functions to determine both the position and orientation of the nanomotor.

The residual of this fit is obtained to isolate the nanoparticle. This brightest and largest feature in this residual ROI is fit to a two-dimensional, radially symmetric Gaussian function to obtain the nanoparticle position. Details of this analysis are presented in the Supporting Information.

Nanoparticles and nanomotors are then tracked between multiple frames of a video. The nanomotor position as a function of time data is fit to a linear function to extract the average value of V_m in the image plane. To extract average values of U_θ and R and from the microvortex advection of a nanoparticle around a nanomotor, the measured trajectory is modeled as a sinusoidal function, as shown in Figure S3, projecting circular motion in three dimensions to images in two dimensions and assuming constant U_θ and R for microvortex advection, at large enough Br. Details of this analysis are presented in the Supporting Information.

In these analyses, measurement uncertainties are determined as the standard uncertainties of the fitted values of position, orientation, and speed and are propagated throughout the algorithm and subsequent calculations. Nanomotors and nanoparticles are localized with typical standard uncertainties of $\approx$ 50 nm and $\approx$ 100 nm, respectively. Limited photon count and motion blur both contribute uncertainty to localization and tracking.

Independently of hydrodynamic interactions with nanomotors, we analyze the stochastic diffusion of nanoparticles before, during, and after acoustic actuation. We localize individual nanoparticles over 500 frames and compute the two-dimensional mean squared displacement (MSD) as a function of time. We measure D from the slope of a linear fit to MSD(t) for individual nanoparticles. We then use the known value of the nanoparticle radius c and the known lumped parameter of $T/(\eta(T))$ for water[43] with the Stokes–Einstein relation to estimate an aqueous solution temperature of $T = (295 \pm 5)$ K (average $\pm$ standard uncertainty) before, during, and after acoustic actuation. This value is consistent with the ambient experimental temperature of $\approx$ 295 K.

Conflict of Interest: The authors declare no competing financial interest.

Acknowledgment. A.L.B., L.O.M., P.P.M., and P.N.P. acknowledge support of this research under the Cooperative Research Agreement between the University of Maryland and the National Institute of Standards and Technology Center for Nanoscale Science and Technology, Award 70NANB10H193, through the University of Maryland. W.W., S.A., and T.M. acknowledge support of this research by the Penn State Materials Research Science and Engineering Center (MRSEC), under NSF grant DMR-0820404. The authors gratefully acknowledge W. Saslow, M. Stiles, and J. Fagan for helpful discussions and insightful reviews.

Supporting Information Available: Details of simplifying assumptions, perturbation estimates, image analysis, tracking analysis, and representative videos are available free of charge *via* the Internet at http://pubs.acs.org.

Note Added after ASAP Publication: This manuscript was published ASAP on July 14, 2014. A correction was made to the caption of Figure 2 and the revised version was reposted on July 16, 2014.

REFERENCES AND NOTES

1. Friend, J.; Yeo, L. Y. Microscale Acoustofluidics: Microfluidics Driven *via* Acoustics and Ultrasonics. *Rev. Mod. Phys.* **2011**, *83*, 647–704.
2. Wang, W.; Castro, L. A.; Hoyos, M.; Mallouk, T. E. Autonomous Motion of Metallic Microrods Propelled by Ultrasound. *ACS Nano* **2012**, *6*, 6122–6132.
3. Paxton, W. F.; Kistler, K. C.; Olmeda, C. C.; Sen, A.; St. Angelo, S. K.; Cao, Y.; Mallouk, T. E.; Lammert, P. E.; Crespi, V. H. Catalytic Nanomotors: Autonomous Movement of Striped Nanorods. *J. Am. Chem. Soc.* **2004**, *126*, 13424–13431.
4. Demirok, U. K.; Laocharoensuk, R.; Manesh, K. M.; Wang, J. Ultrafast Catalytic Alloy Nanomotors. *Angew. Chem., Int. Ed.* **2008**, *47*, 9349–9351.
5. Sailapu, S. K.; Chattopadhyay, A. Induction of Electromotive Force by an Autonomously Moving Magnetic Bot. *Angew. Chem., Int. Ed.* **2014**, *53*, 1521–1524.
6. Lee, T.-C.; Alarcón-Correa, M.; Miksch, C.; Hahn, K.; Gibbs, J. G.; Fischer, P. Self-Propelling Nanomotors in the Presence of Strong Brownian Forces. *Nano Lett.* **2014**, *14*, 2407–2412.
7. Ghosh, A.; Fischer, P. Controlled Propulsion of Artificial Magnetic Nanostructured Propellers. *Nano Lett.* **2009**, *9*, 2243–2245.
8. Gao, W.; Kagan, D.; Pak, O. S.; Clawson, C.; Campuzano, S.; Chuluun-Erdene, E.; Shipton, E.; Fullerton, E. E.; Zhang, L.; Lauga, E. Cargo-Towing Fuel-Free Magnetic Nanoswimmers for Targeted Drug Delivery. *Small* **2012**, *8*, 460–467.
9. Kim, K.; Xu, X.; Guo, J.; Fan, D. L. Ultrahigh-Speed Rotating Nanoelectromechanical System Devices Assembled from Nanoscale Building Blocks. *Nat. Commun.* **2014**, 5.
10. Wang, W.; Li, S.; Mair, L.; Ahmed, S.; Huang, T. J.; Mallouk, T. E. Acoustic Propulsion of Nanorod Motors Inside Living Cells. *Angew. Chem., Int. Ed.* **2014**, *126*, 3265–3268.
11. Dong, B.; Zhou, T.; Zhang, H.; Li, C. Y. Directed Self-Assembly of Nanoparticles for Nanomotors. *ACS Nano* **2013**, *7*, 5192–5198.
12. Garcia-Gradilla, V.; Orozco, J.; Sattayasamitsathit, S.; Soto, F.; Kuralay, F.; Pourazary, A.; Katzenberg, A.; Gao, W.; Shen, Y. F.; Wang, J. Functionalized Ultrasound-Propelled Magnetically Guided Nanomotors: Toward Practical Biomedical Applications. *ACS Nano* **2013**, *7*, 9232–9240.
13. Ju, H.; Zhang, X.; Wang, J. Nanobiosensing for Clinical Diagnosis. In *NanoBiosensing*; Springer: Berlin, 2011; pp 535–567.
14. Wang, J. Can Man-Made Nanomachines Compete with Nature Biomotors? *ACS Nano* **2009**, *3*, 4–9.
15. Mornet, S.; Vasseur, S.; Grasset, F.; Duguet, E. Magnetic Nanoparticle Design for Medical Diagnosis and Therapy. *J. Mater. Chem.* **2004**, *14*, 2161–2175.
16. Perez, J. M.; Simeone, F. J.; Saeki, Y.; Josephson, L.; Weissleder, R. Viral-Induced Self-Assembly of Magnetic Nanoparticles Allows the Detection of Viral Particles in Biological Media. *J. Am. Chem. Soc.* **2003**, *125*, 10192–10193.
17. Patra, D.; Sengupta, S.; Duan, W.; Zhang, H.; Pavlick, R.; Sen, A. Intelligent, Self-Powered, Drug Delivery Systems. *Nanoscale* **2013**, *5*, 1273–1283.
18. Nair, B. G.; Nagaoka, Y.; Morimoto, H.; Yoshida, Y.; Maekawa, T.; Kumar, D. S. Aptamer Conjugated Magnetic Nanoparticles as Nanosurgeons. *Nanotechnology* **2010**, *21*, 455102.
19. Chwang, A. T.; Wu, T. Y. Hydromechanics of Low-Reynolds-Number Flow. Part 1. Rotation of Axisymmetric Prolate Bodies. *J. Fluid Mech.* **1974**, *63*, 607–622.
20. Silverman, M.; Simon, M. Flagellar Rotation and the Mechanism of Bacterial Motility. *Nature* **1974**, *249*, 73–74.
21. Peyer, K. E.; Zhang, L.; Nelson, B. J. Localized Non-Contact Manipulation Using Artificial Bacterial Flagella. *Appl. Phys. Lett.* **2011**, *99*, 174101.
22. Latham, A. H.; Williams, M. E. Controlling Transport and Chemical Functionality of Magnetic Nanoparticles. *Acc. Chem. Res.* **2008**, *41*, 411–420.
23. Chong, W. H.; Chin, L. K.; Tan, R. L. S.; Wang, H.; Liu, A. Q.; Chen, H. Stirring in Suspension: Nanometer-Sized Magnetic Stir Bars. *Angew. Chem.* **2013**, *125*, 8732–8735.
24. Xi, W.; Solovev, A. A.; Ananth, A. N.; Gracias, D. H.; Sanchez, S.; Schmidt, O. G. Rolled-up Magnetic Microdrillers: Towards Remotely Controlled Minimally Invasive Surgery. *Nanoscale* **2013**, *5*, 1294–1297.
25. Solovev, A. A.; Xi, W.; Gracias, D. H.; Harazim, S. M.; Deneke, C.; Sanchez, S.; Schmidt, O. G. Self-Propelled Nanotools. *ACS Nano* **2012**, *6*, 1751–1756.
26. Goldowsky, J.; Mastrangeli, M.; Jacot-Descombes, L.; Gullo, M. R.; Mermoud, G.; Brugger, J.; Martinoli, A.; Nelson, B.; Knapp, H. F. Acousto-Fluidic System Assisting In-Liquid Self-Assembly of Microcomponents. *J. Micromech. Microeng.* **2013**, *23*, 125026.
27. Sinn, I.; Albertson, T.; Kinnunen, P.; Breslauer, D. N.; McNaughton, B. H.; Burns, M. A.; Kopelman, R. Asynchronous Magnetic Bead Rotation Microviscometer for Rapid, Sensitive, and Label-Free Studies of Bacterial Growth and Drug Sensitivity. *Anal. Chem.* **2012**, *84*, 5250–5256.
28. Bruus, H. Acoustofluidics 7: The Acoustic Radiation Force on Small Particles. *Lab Chip* **2012**, *12*, 1014–1021.

29. Guasto, J. S.; Johnson, K. A.; Gollub, J. P. Oscillatory Flows Induced by Microorganisms Swimming in Two Dimensions. *Phys. Rev. Lett.* **2010**, *105*, 168102.
30. Miño, G.; Dunstan, J.; Rousselet, A.; Clément, E.; Soto, R. Induced Diffusion of Tracers in a Bacterial Suspension: Theory and Experiments. *J. Fluid Mech.* **2013**, *729*, 423–444.
31. Magdanz, V.; Sanchez, S.; Schmidt, O. G. Development of a Sperm-Flagella Driven Micro-Bio-Robot. *Adv. Mater.* **2013**, *25*, 6581–6588.
32. Petit, T.; Zhang, L.; Peyer, K. E.; Kratochvil, B. E.; Nelson, B. J. Selective Trapping and Manipulation of Microscale Objects Using Mobile Microvortices. *Nano Lett.* **2011**, *12*, 156–160.
33. Diller, E.; Ye, Z.; Sitti, M. Rotating Magnetic Micro-Robots for Versatile Non-Contact Fluidic Manipulation of Micro-Objects. In *2011 IEEE/RSJ International Conference on Intelligent Robots and Systems*; IEEE: New York, **2011**; pp 1291−1296.
34. Happel, J.; Brenner, H. *Low Reynolds Number Hydrodynamics*; Prentice Hall: NJ, 1965.
35. Lierke, E. G. Acoustic Levitation - A Comprehensive Survey of Principles and Applications. *Acustica* **1996**, *82*, 220–237.
36. Landau, L. D.; Lifshitz, E. M. *Fluid Mechanics*; Pergamon Press: Oxford, 1987.
37. Liu, L.; Yoo, S. H.; Lee, S. A.; Park, S. Wet-Chemical Synthesis of Palladium Nanosprings. *Nano Lett.* **2011**, *11*, 3979–3982.
38. Tottori, S.; Zhang, L.; Qiu, F. M.; Krawczyk, K. K.; Franco-Obregon, A.; Nelson, B. J. Magnetic Helical Micromachines: Fabrication, Controlled Swimming, and Cargo Transport. *Adv. Mater.* **2012**, *24*, 811–816.
39. Peyer, K. E.; Tottori, S.; Qiu, F. M.; Zhang, L.; Nelson, B. J. Magnetic Helical Micromachines. *Chem.—Eur. J.* **2013**, *19*, 28–38.
40. Li, J.; Sattayasamitsathit, S.; Dong, R.; Gao, W.; Tam, R.; Feng, X.; Ai, S.; Wang, J. Template Electrosynthesis of Tailored-Made Helical Nanoswimmers. *Nanoscale*, in press.
41. Xu, J.; Wang, H.; Liu, C.; Yang, Y.; Chen, T.; Wang, Y.; Wang, F.; Liu, X.; Xing, B.; Chen, H. Mechanical Nanosprings: Induced Coiling and Uncoiling of Ultrathin Au Nanowires. *J. Am. Chem. Soc.* **2010**, *132*, 11920–11922.
42. Martin, B. R.; Dermody, D. J.; Reiss, B. D.; Fang, M. M.; Lyon, L. A.; Natan, M. J.; Mallouk, T. E. Orthogonal Self-Assembly on Colloidal Gold-Platinum Nanorods. *Adv. Mater.* **1999**, *11*, 1021–1025.
43. Kestin, J.; Sokolov, M.; Wakeham, W. A. Viscosity of Liquid Water in the Range 8 to 150 C. *J. Phys. Chem. Ref. Data* **1978**, *7*, 941–948.